# 12.4 Gravity waves trapped under the leading anvil of an MCS during BAMEX

Benjamin C. Baranowski* and Matthew D. Parker
North Carolina State University, Raleigh, North Carolina
Brandon A. Storm,
Texas Tech University, Lubbock, Texas

## 1 Introduction

Gravity waves are common features in and around deep moist convection. These gravity waves are dispersive and act in response to vertical fluctuations in heating and momentum caused by the convection. Two general types of waves can be generated by these fluctuations: Low frequency modes and high frequency modes (Mapes 1993; Fovell et al. 2006, hereafter referred to as F06). The low frequency waves result from the slow, consistent release of latent heat associated with the mesoscale structure of the convection. Sporadic variations in this heating within the convective cells result in the high frequency waves. The low frequency waves are hydrostatic; therefore, their energy cannot propagate vertically. The high frequency waves are not hydrostatic so their energy can propagate vertically.

In many situations, the energy from these high frequency waves simply passes through the troposphere and into the stratosphere. However, if the vertical profiles of stability and wind shear are favorable, trapping or ducting of the waves can occur. Fovell (2002) and others showed that the low frequency waves and other mesoscale circulations can aid in producing favorable profiles for wave trapping in the pre-squall line environment. This pre-line trapping is very similar to the trapping of gravity waves by the trailing anvil described by Yang and Houze (1995). Trapping of these high frequency waves can have implications for storm propagation and subsequent storm initiation (F06).

F06 showed that the warm moist inflow layer can be modified by the low frequency waves. The absolute humidity of the inflow layer can be increased which increases the convective available potential energy (CAPE). As the high frequency waves are generated, they begin to propagate vertically but can be reflected allowing the wave energy to remain in the troposphere. Lindzen and Tung (1976) provided a detailed discussion of a variety of ways mesoscale gravity waves can become trapped or ducted in the troposphere. If the high frequency waves can remain in the troposphere, they can affect the propagation and evolution of the convective line (i.e. discrete propagation events as described by F06).

The lack of in-situ measurements around strong convection has required studies like those mentioned above to rely heavily upon numerical models. Past idealized simulations of squall lines with leading stratiform precipitation have shown roll features (e.g. Fig. 1) that were originally thought to be an artifact of the 2D model geometry (e.g. that used by Parker and Johnson (2004)). However, other modeling results (e.g., F06; Tripoli and Cotton 1989a; Tripoli and Cotton 1989b) have shown similar roll features trapped beneath the leading anvil suggesting these features are not a numerical artifact.

During the 31 May 2003, Bow Echo and Mesoscale Convective Vortex Experiment (BAMEX, Davis et al. 2004) event, a front fed, leading stratiform (FFLS) squall line (Parker and Johnson 2004) was sampled by an array of mea-

* *Corresponding author address:* Benjamin C. Baranowski, Department of Marine, Earth, & Atmospheric Sciences, North Carolina State University, Campus Box 8208, Raleigh, NC 27695–8208. E-mail: bcbarano@ncsu.edu

suring platforms. Wind fields retrieved from two airborne Doppler radars show roll features similar to those in the numerical simulations (Fig. 2, x $\approx$ 27 km). The existence of the rolls provides the first observational evidence of what may be gravity waves trapped below the leading anvil of a squall line. Unfortunately, the time required for each aircraft flight leg was too long (approximately 20 minutes) to easily track the rolls and verify, using specific wave characteristics, that the features are gravity waves. Thus, numerical simulations, initialized with observations, are included in this study to overcome this deficiency.

# 2 Data, Methods and Event Summary

## 2.1 Event Summary

Supercell thunderstorms formed over Wisconsin around 2130 UTC on 30 May. As these storms moved southeastward, the generation of a precipitation cooled outflow initiated new convection and the system transitioned to a FFLS MCS by 0200 UTC 31 May (Fig. 3). The gravity wave features to be investigated occurred during this mature MCS stage between 0200 UTC and 0330 UTC. Despite the reduced instability over eastern Illinois and western Indiana (not shown), the FFLS system continued to move east/southeastward until approximately 0400 UTC (Fig. 3) when the system finally decayed.

## 2.2 Observational Data

This study uses airborne Doppler radar and ground based radiosonde data collected during BAMEX. Two vertically scanning, X-band (3.2 cm wavelength) Doppler radars were used to sample the convective system. Individual flight legs the each aircraft ranged between 10 and 30 minutes. The ground based radiosondes were released hourly ahead of the convective line. For information concerning the dual Doppler synthesis and radar data editing see Storm (2005) and Storm et al. (2007).

## 2.3 Numerical Simulation Setup

The Weather Research and Forecasting (WRF) model, using the Advanced Research WRF (ARW) physics core version 2.2 is used for the numerical simulation. The WRF Preprocessing System (WPS) is used to produce initial and boundary conditions using the North American Regional Reanalysis (NARR) data. The simulation is run in three dimensions on a domain of 800 km $\times$ 1000 km in the east-west and north-south directions, respectively (figure 4). The horizontal grid spacing is one km. 29 stretched vertical levels are used, with highest resolution near the surface and an average vertical grid spacing of 500 m. Radiation, surface flux and boundary layer processes are included as well as the WRF Single-Moment 6 (Hong et al. 2004) microphysics scheme which includes graupel. The simulation is run for six hours with the model boundaries being updated by the NARR data every three hours.

# 3 Results

## 3.1 WRF Simulation

The simulated squall line produced by the WRF model has many of the same characteristics as the observed squall line. By 0300 UTC, a mature FFLS squall is located in northern Indiana, displaced approximately 150 km north of the observed squall line (Fig. 5a). Similar to the observed case, the WRF squall line has an overturning updraft and leading stratiform precipitation region. Both these features are common to other observed FFLS squall lines (Parker and Johnson 2004). The simulation also produced precipitation to the east and north of the main squall line, much as was observed in central Indiana and southern Michigan (Fig. 5).

Although the WRF simulation doesn't reproduce the squall line identically, we feel the similarities in location, timing and storm type justify using this WRF simulation to further analyze the squall line and the gravity waves. Also, given the above similarities, we feel general conclusions garnered from the WRF simulation can be credibly applied to the observed case.

### 3.2 Trapped Gravity Waves

Similar to results shown by F06, regions of ascent and enhanced reflectivity are present in the observed dual Doppler wind and reflectivity fields downshear of the main convective region (Fig. 2). These regions of ascent are postulated to be cut-off updrafts that take the form of gravity waves (buoyancy rolls) underneath the leading anvil. Unlike the F06 simulations, the gravity waves in the observed case do not result in discrete propagation.

However, the waves produced in the WRF simulation are very similar to the observed features (Fig. 5b at 87W and 86.9W). The simulated waves occur under the leading anvil between 4 km and 7 km in height which also matches well with the observations. Although the visual aspects of both the observed and simulated rolls suggest the features are gravity waves, an analysis of the pre-line environment is necessary to determine if the atmosphere is capable of trapping such waves in the forward anvil.

### 3.3 Pre-line Trapping Mechanisms

Reflection or refraction of gravity waves in a layer can occur if the Scorer parameter $l^2$ is less than the horizontal wave number of the gravity wave ($l^2 - k^2 < 0$), or if a sharp decrease in $l^2$ occurs with height. Similarly, if two such layers exist, gravity waves can become trapped between them (Durran and Klemp 1982). The Scorer parameter (Scorer 1949) for the pre-line region is defined as:

$$l^2 \approx \frac{N_*^2}{(U-c)^2} - \frac{1}{(U-c)}\frac{d^2U}{dz^2} \qquad (1)$$

where $N_*^2$ is the subsaturated (N) or saturated $N_m$ Brunt-Väisälä frequency (Durran and Klemp 1982, their equation 5), U is the line normal wind speed and c is the wave phase speed. The calculation of $N_m$ requires the profile of total water mixing ratio, which has to be estimated from the observed radar data. For the model simulation, the total water mixing ratio is easily calculated from the microphysics scheme.

The observed pre-line Scorer profile is generated by combining the Glass sounding (G1 from figure 3) released at 0329 UTC and a wind profile derived from the dual Doppler analysis at 0250 UTC. The observed pre-line profile of $l^2$ (Fig. 6a) shows that wave trapping can occur between 2.5 km and 10 km. The roll features identified in the dual Doppler analysis occur around 6 km (Fig. 2). Likewise, waves can become trapped between the 2 and 8 km in the simulated environment (Fig. 6b). In both cases, the trapping layers are characterized by weak static stability and strong, line-perpendicular winds (not shown).

The Scorer method described above is typically applied to topographic waves where a sinusoidal ridge (or series of ridges) is used to force waves. Lindzen and Tung (1976) (hereafter referred to as LT76) provide ways in which gravity waves can be trapped in other ways than that described above. Most relevant to this study is ducting of waves by a conditionally unstable layer with shear but without a steering level. As the speed of the mean flow approaches the intrinsic windspeed, the amount of reflection increases. Although the present profiles do not have true critical levels, they do have layers in which both the stability and U-c are very small. Given this, some reflection and refraction of gravity waves is likely occurring under the leading anvil. Notably, where $\mid U - c \mid$, and $l^2 \rightarrow \infty$such that the layers where the LT76 mechanism is active corresponds to layers of large vertical change in $l^2$ (see Fig. 6).

## 4 Summary

Observations provided by airborne Doppler radars during the BAMEX field project show some of the first observational evidence of gravity waves trapped under the leading anvil of a front-fed leading stratiform squall line. The wave features have typical gravity wave phase speeds and match well with gravity waves produced by numerically simulated convection. Analysis of pre-line profiles of the Scorer parameter show a strong decrease with height near 10 km providing a layer where the waves can become trapped.

The aircraft flight legs were, on average, between 10 and 20 minutes, making tracking of the waves difficult. A numerical simulation, using

the WRF model is used as a proxy to help fill in these gaps. The WRF simulation produces an FFLS squall line similar to that observed and gravity waves are produced by the convection. Analysis of the simulated pre-line profile of the Scorer parameter shows that trapping of waves can occur. Although the WRF simulated squall line is not identical to the observed squall line, the simulated line also produced trapped gravity waves.

The roll features in the dual Doppler wind field during the 31 May 2003 squall line are likely to be trapped gravity waves. This conclusion strengthens Fovell et al.'s claim that gravity waves can exert influence on the forward environment of a squall line and potentially alter the evolution and propagation of the line. The FFLS convective mode appears to be ideally suited for the trapping of such waves.

## References


Durran, D. R. and J. B. Klemp, 1982: The effects of moisture on the Brunt-Väisälä frequency. *J. Atmos. Sci.*, **39**, 2152–2158.

Fovell, R. G., 2002: Upstream influence of numerically simulated squall-line storms. *Quart. J. Roy. Meteor. Soc.*, **128**, 264–278.

Fovell, R. G., G. L. Mullendore, and S. Kim, 2006: Discrete propagation in numerically simulated nocturnal squall lines. *Mon. Wea. Rev.*, **134**, 3735–3752.

Hong, S.-Y., J. Dudhia, and S.-H. Chen, 2004: A revised approach to ice microphysical processes for the bulk parameterization of clouds and precipitation. *Mon. Wea. Rev.*, **132**, 103–102.

Lindzen, R. S. and K.-K. Tung, 1976: Banded convective activity and gravity waves.

Mapes, B. E., 1993: Gregarious tropical convection. *J. Atmos. Sci.*, **50**, 2026–2037.

Parker, M. D. and R. H. Johnson, 2004: Simulated convective lines with leading precipitation. part I: Governing dynamics. *J. Atmos. Sci.*, **61**, 1637–1655.

Scorer, R. S., 1949: Theory of waves in the lee of mountains. *Quart. J. Roy. Meteor. Soc.*, **75**, 41–56.

Storm, B. A., 2005: Investigation of 31 May 2003 MCS with leading stratiform precipitation from BAMEX. Master's thesis, Department of Geosciences, University of Nebraska, Lincoln, Nebraska.

Storm, B. A., M. Parker, and D. Jorgensen, 2007: A convective line with leading stratiform precipitation from BAMEX. *Mon. Wea. Rev.*, **135**, 1769–1785.

Tripoli, G. J. and W. R. Cotton, 1989a: Numerical study of an observed orogenic mesoscale convetive system. part I: Simulated genesis and comparison with observations. *Mon. Wea. Rev.*, **117**, 273–304.

———, 1989b: Numerical study of an observed orogenic mesoscale convetive system. part II: Analysis of governing dynamics. *Mon. Wea. Rev.*, **117**, 305–328.

Yang, M.-J. and R. A. Houze, Jr., 1995: Multicell squall-line structure as a manifestation of vertically trapped gravity waves. *Mon. Wea. Rev.*, **123**, 641–660.

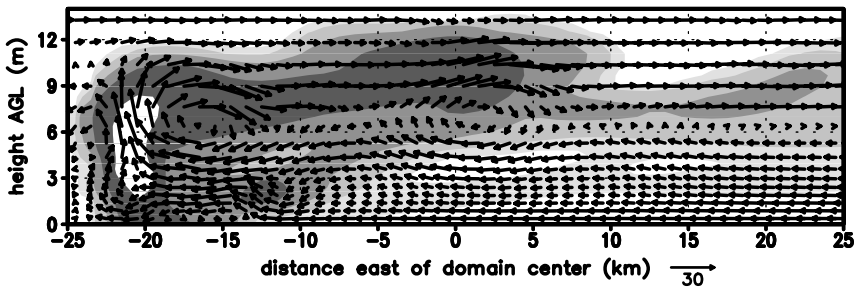


Figure 1: Total hydrometeor mixing ratio (shaded) and wind vectors at t=2 h from the 2D control FFLS simulation of Parker and Johnson (2004).

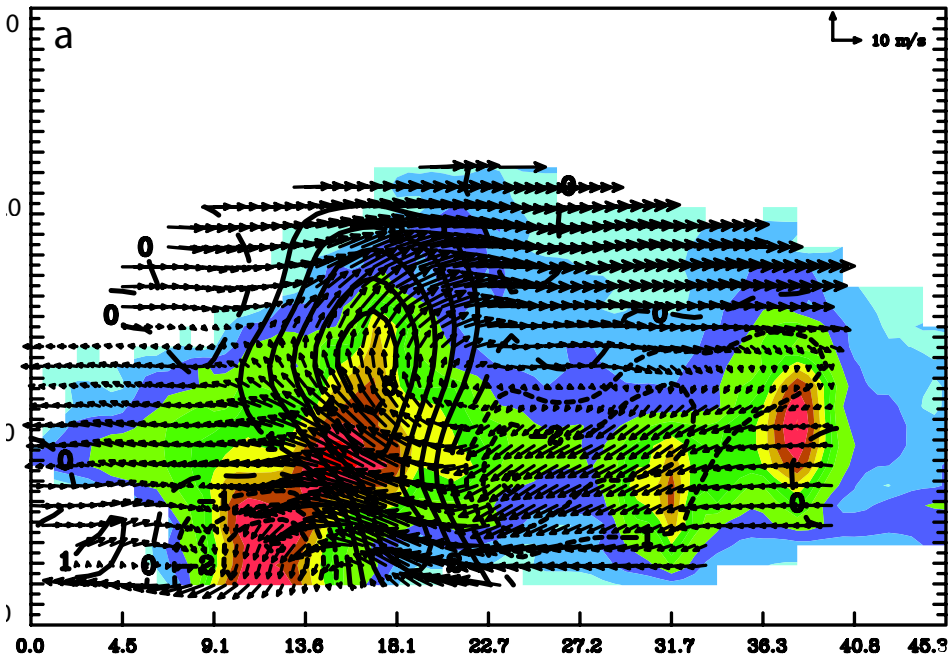


Figure 2: Vertical cross-sections of reflectivity (shaded), vertical velocity (contoured) and storm relative winds at 0300 UTC. The vertical axis is heights MSL (km) and the horizontal axis is distance along the cross-section (km). Cross section position shown in Fig. 3.

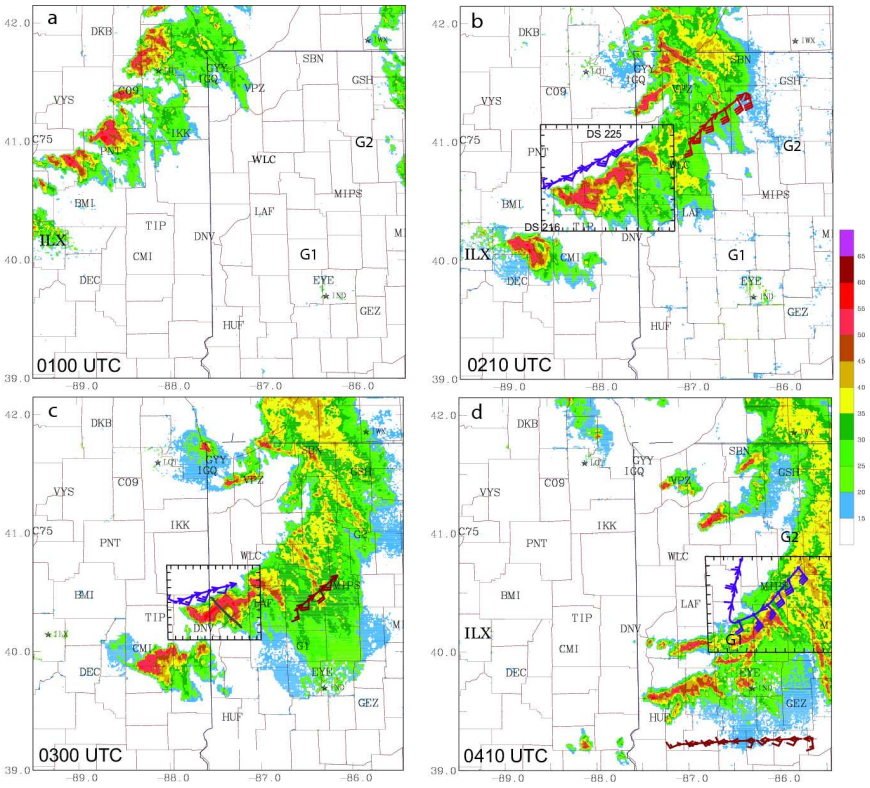


Figure 3: Composite radar reflectivity (dBZ) from WSR-88D radars and flight paths for flight legs (purple and red lines): (a) 0100 UTC, (b) 0210 UTC, (c) 0300 UTC, (d) 0410 UTC. Grey line in (c) identifies the cross section location shown in Fig. The location of the Glass sounding is shown as G1.2.

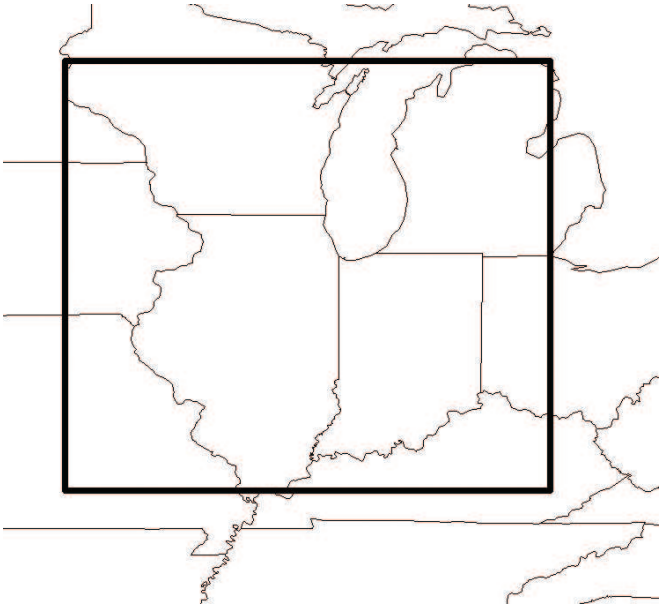

Figure 4: Computational domain for the WRF simulation

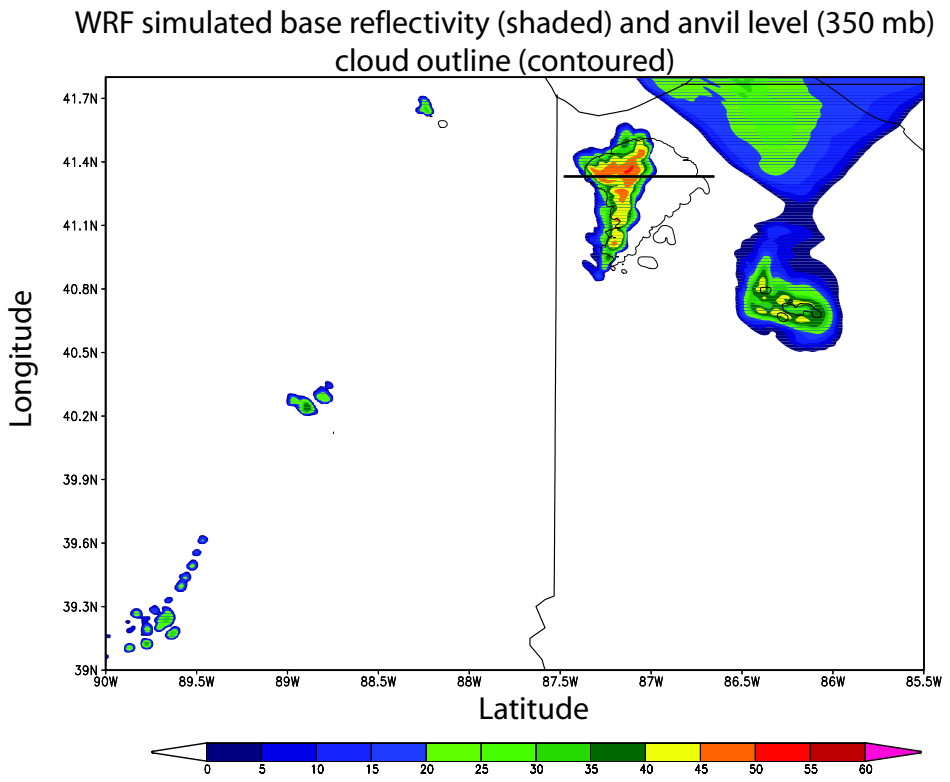


(a)

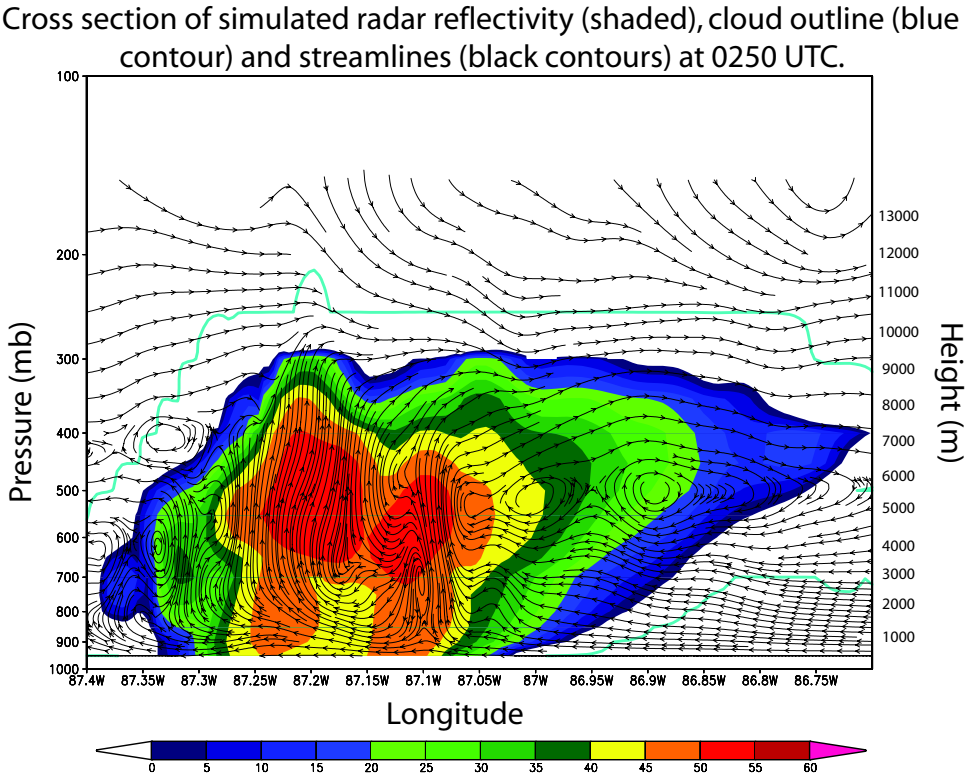


(b)



Figure 5: (a) WRF simulated base reflectivity and anvil level cloud outline at 0250 UTC. (b) Cross-section through latitude = 41.3 (solid line indicated on (a)) of radar reflectivity (shaded), cloud outline and streamlines.

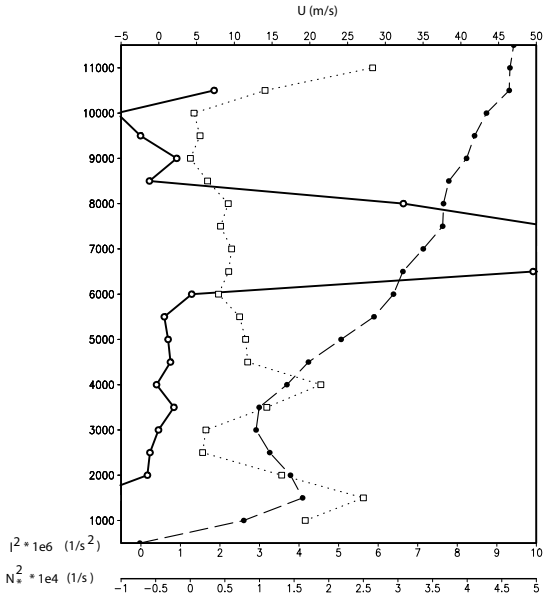


(a)

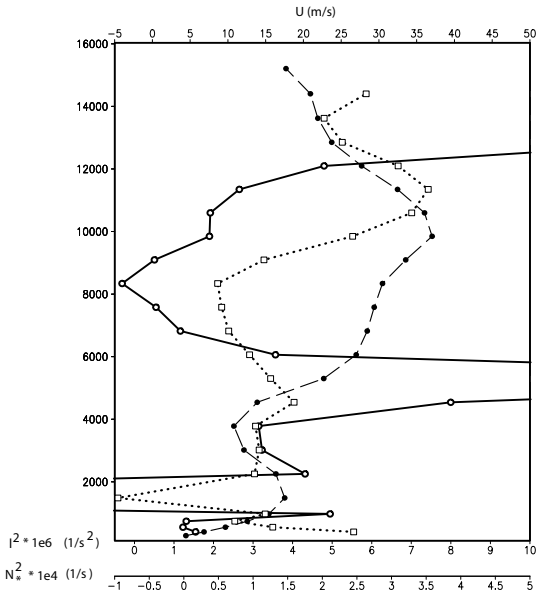


(b)

Figure 6: Profiles of Scorer parameter (solid line), line-perpendicular winds (dashed line) and Brunt-Väisälä frequency (dotted line) for the observed case (a) and the WRF simulation (b).